Earth Syst. Sci. Data Discuss., 6, 513–540, 2013
www.earth-syst-sci-data-discuss.net/6/513/2013/
doi:10.5194/essdd-6-513-2013

Open Access Earth System Science Data Discussions

Atmospheric ozone above Troll station, Antarctica observed by a ground based microwave radiometer

M. Daae[1,2], C. Straub[1,3], P. J. Espy[1,2], and D. A. Newnham[4]

[1]Norwegian University of Science and Technology, Department of Physics, Trondheim, Norway
[2]Birkeland Centre for Space Science, Bergen, Norway
[3]Institute of Applied Physics, University of Bern, Bern, Switzerland
[4]British Antarctic Survey, Cambridge, UK

Received: 6 August 2013 – Accepted: 28 August 2013 – Published: 5 September 2013

Correspondence to: M. Daae (marianne.daae@ntnu.no)

Published by Copernicus Publications.

Abstract

This paper describes the stratospheric and mesospheric ozone profiles retrieved from spectral measurements of the 249.96 GHz O_3 line, using the British Antarctic Survey's ground-based Microwave Radiometer at Troll (BAS-MRT), Antarctica (72°01′ S, 02°32′ E, 62° Mlat). The instrument operated at Troll from February 2008 through January 2010, and hourly averaged spectra were used to retrieve approximately 22 ozone profiles per day. The ozone profiles cover the pressure range from 3 to 0.02 hPa (approximately 38 to 72 km) which includes the topside of the stratospheric ozone layer and the peak of the tertiary maximum. Comparing the retrieved ozone volume mixing ratio (vmr) values to Aura/MLS and SD-WACCM shows no significant bias to within the instrumental uncertainties. The long-term variations (> 20 days) between MLS and SD-WACCM agree well with BAS-MRT at all altitudes with significant correlation coefficients of at least 0.9 (0.7 with SD-WACCM) in the upper stratosphere and middle mesosphere. A weaker correlation is found for the long-term variations in summer when most of the vmr values are below the random noise level of Aura/MLS. The correlation of short-term variations (< 20 days) between MLS and BAS-MRT agree well at all altitudes with significant correlation coefficients of at least 0.7 in the upper stratosphere and middle mesosphere. The ozone profiles retrieved at Troll, Antarctica extend the sparse data coverage of middle atmospheric ozone above Antarctica, where, due to the dynamic nature of the ozone concentrations, systematic observations with a high temporal resolution are desirable. The O_3 profiles presented here are stored at the UK's Polar Data Centre (http://doi.org/nc3) and are available for public scientific use.

1 Introduction

Ozone concentrations in the middle atmosphere are governed by UV photolysis of O_2, O_3 and H_2O, and catalytic cycles involving odd hydrogen (HO_x = H, OH, HO_2). The stratospheric ozone maximum near 30 km is associated with near- and mid-ultraviolet

(UV) photo-dissociation of O_2 followed by recombination. The secondary maximum near the mesopause (Hays and Roble, 1973) results from the downward transport and recombination of O associated with Far-UV (FUV) dissociation of O_2 in the lower thermosphere. Between these two maxima in the summer, the availability of HO_x results in a deep minimum in the mesospheric ozone abundance. However, during winter near the polar-night terminator, a tertiary maximum occurs near 70 km where H_2O is no longer efficiently dissociated into odd hydrogen due to high optical depths in the FUV (Marsh et al., 2001). This ozone peak in the middle mesosphere can be observed from early fall until late spring, extending approximately 30° in latitude from the equatorward edge of the polar-night terminator (Hartogh et al., 2004).

Ozone in the middle mesosphere undergoes a strong diurnal cycle as the odd oxygen is cycled between O during the day and O_3 at night. The resulting ozone mixing ratio can go from close to 0 ppmv during the day and reach 3–4 ppmv in the course of a few hours during twilight. Planetary waves, tides and gravity waves also cause variations in the tertiary maximum as indicated by Hartogh et al. (2004). Space weather effects can cause significant loss of O_3 throughout the middle atmosphere (e.g. Solomon et al., 1982; Jackman et al., 2009; Daae et al., 2012). This can occur by direct precipitation of charged particles into the mesosphere that increase NO_x levels by up to 2.6 gigamoles per year (e.g. Turunen et al., 2009; Randall et al., 2006) and enhance HO_x levels by 100 % (e.g. Verronen et al., 2011), locally depressing O_3 levels due to catalytic reactions.

Ground-based observations of O_3 in the mesosphere using microwave radiometry have been primarily located in the Northern Hemisphere (e.g. Muscari et al., 2012; Palm et al., 2010). Hartogh et al. (2004), using the 142 GHz O_3 line in northern Norway (69.29° N, 10.13° E), observed large ozone variations within the 1995–1996 winter season, which they attributed to modulations of the dynamics controlling the availability of H_2O. Sonnemann et al. (2007) used a microwave technique at Lindau, Germany (51.66° N, 10.13° E) to analyze the night-to-day ratio of ozone in the mesosphere. They

ESSDD
6, 513–540, 2013

Atmospheric ozone above Troll station, Antarctica measured by BAS-MRT

M. Daae et al.

found that while night-time ozone levels are enhanced due to a west-wind regime, the daytime ozone is less influenced by the zonal wind.

Ground-based radiometer observations of ozone in the Southern Hemisphere are sparse with systematic observations only at mid-latitudes in New Zealand and South America (McDermid et al., 1998; Orte et al., 2011), and from Antarctica during the years 1993, 1995 and 1999 (Nemuc and De Zafra, 2007). Here we describe nearly two years of continuous ground-based radiometer measurements of ozone above Troll, Antarctica (72°01′ S, 02°32′ E, 1270 m above sea level) covering the upper stratosphere and lower mesosphere. The instrument, as well as its location within the polar vortex and at high geomagnetic latitude (62° Mlat, $L = 4.76$), allows both short- and long-term chemical and dynamical variations as well as the impact on the O_3 from charged particle precipitation to be studied (Newnham et al., 2011; Daae et al., 2012; Demissie et al., 2013).

2 Measurement

The British Antarctic Survey's Microwave Radiometer at Troll (BAS-MRT) measures spectral regions around the rotational transitions of nitric oxide (NO) at 250.796 GHz (Newnham et al., 2011), carbon monoxide (CO) at 230.538 GHz (Straub et al., 2013) and ozone (O_3) at 249.96 GHz. The O_3 observations, and the retrieved altitude profiles, are presented here.

2.1 Instrument and calibration

BAS-MRT observes at an azimuth angle of 288° and a zenith angle of 60°, which is in the direction toward the SANAE research station as seen in Fig. 1. The instrument field of view intercepts altitudes of 40, 60 and 80 km at geographical locations (71.81° S, 0.58° E), (71.71° S, 0.37° W) and (71.62° S, 1.33° W), respectively.

ESSDD
6, 513–540, 2013

The instrument consists of a cryogenically cooled radiometric front-end coupled to a spectrometer backend. In the front-end heterodyne receiver, the incoming radiation is combined with an independent local oscillator signal at 255.6 GHz by a Superconductor-Insulator-Superconductor mixer cooled to 4 K. The intermediate frequency (IF) signal in the 4 to 6 GHz range is then amplified. For O_3 measurements the signal is further down-converted to 2.1 GHz and analyzed using a Chirp Transform Spectrometer (CTS) (Hartogh and Hartmann, 1990; Villanueva and Hartogh, 2004; Villanueva et al., 2006) with a 28 kHz resolution and 220 MHz bandwidth.

A three-way chopper system selects the microwave emission either from the atmosphere, a 60 K cold calibration load or a room temperature hot calibration load and directs it into the main receiver. The atmospheric signal is then calibrated using the switching technique of Dicke and Beringer (1946) as described by Parrish (1994, and references therein). The signal from each target is integrated by the spectrometer for 8 s, resulting in a calibrated O_3 spectrum every 17.5 s. Further details about the radiometer and its measurements can be found in Espy et al. (2006) and Straub et al. (2013).

The O_3 signal is modified by absorption and emission due to other atmospheric species, predominantly in the troposphere by water vapor, and needs to be accounted for. A tropospheric correction factor for the spectra is calculated as described in Forkman et al. (2012).

2.2 Dataset

BAS-MRT made observations corresponding to the data presented in this paper from February 2008 through January 2010. On average, the O_3 line was observed for approximately 20 h each day, as around 12:00 UTC (GMT) the frequency of the local oscillator was manually changed and the instrument observed CO for two hours (Straub et al., 2013). To increase the Signal to Noise (S/N), O_3 spectra are integrated for one hour (typically 203 spectra). In the retrieval of the O_3 profile we only consider integrated spectra with a noise level lower than 0.71 K. Figure 2 shows example O_3-spectra for

ESSDD
6, 513–540, 2013

summer noon and winter midnight, and indicates the spectral region used in the retrievals described below as well as the variable instrumental baseline.

3 Retrieval of vertical profiles

The spectra are inverted into altitude profiles using an iterative optimal estimation method (Rodgers, 2004) implemented in the Qpack (v. 7.4) software package (Eriksson et al., 2005). The forward model, Atmospheric Radiative Transfer Simulator 2 (ARTS 2 v. 2.1.459), handles the radiative transfer through the atmosphere for given species and instrument configuration (Eriksson et al., 2011).

3.1 Retrieval set-up

As may be seen in Fig. 2, the spectra contain the pressure- and Doppler- broadened O_3 thermal emission line, and also a frequency dependent baseline that originates from standing waves in the front end of the radiometer. Thus, the retrieved quantities in the inversion are O_3 volume mixing ratio (vmr), instrumental baseline and atmospheric temperature. The O_3 vmr is inverted from a 40 MHz section of the spectrum centered on the 249.96 GHz O_3 line. The baseline is approximated by a 1st order polynomial and the largest spectral component of the baseline, a 78.5 MHz period sinusoid. Testing of the baseline fit over this spectral range shows that these two components ensured optimal retrieval of the baseline without affecting the O_3 vmr values at lower altitudes. To avoid fitting potentially small and time-varying baseline features, the noise threshold on the spectra is set to 0.4 K (0.9 % of the average peak value). Spectroscopic parameters for the forward modeling of the 249.96 GHz O_3 line are taken from the HITRAN 2008 Molecular Spectroscopic Database (Rothman et al., 2009).

The O_3 vmr profiles are retrieved on a pressure grid corresponding to altitude levels from 15 to 120 km with a 2 km spacing, where hydrostatic equilibrium is assumed for the altitude and pressure. The a priori for the atmospheric temperature and O_3 profiles are

ESSDD
6, 513–540, 2013

taken from the Whole Atmosphere Community Climate Model with Specified Dynamics (SD-WACCM) version 3.5.48 (Garcia et al., 2007; Marsh, 2011; Lamarque et al., 2012). The a priori temperatures are the monthly means of a 20 yr climatology, and the a priori of the O_3 profiles are monthly means of a 4 yr climatology (2004–2008). The a prioris are centered at the middle of each month, and intermediate values are linearly interpolated. To account for the diurnal cycle in the O_3 we use day- and night- a priori depending on whether the solar elevation angle is above, or below 0°. The diagonal elements in the covariance of the O_3 a priori are fixed at 0.09 ppmv^2, a value that is comparable to the mean of the variance in the O_3 given by SD-WACCM. The shape of the covariance is set to linearly decrease toward the off-diagonal elements with a correlation length of 0.2 equivalent to a fifth of a pressure decade (about 3 km).

3.2 Results of the retrievals

The retrieval of the O_3 spectra resulted in 13 648 profiles covering 675 days with an average of about 20 profiles per day. Figure 3a shows examples from the results of the O_3 retrievals and indicates the good quality of the spectral fits. The residuals shown in Fig. 3b are below the noise threshold of 0.4 K that was set for the spectra.

The Averaging Kernels (AVK) for each retrieved altitude are shown in Fig. 3c, describing the relationship between the true, a priori-, and retrieved- states of the atmosphere (Rodgers, 2004). AVK's indicate the range of altitudes over which the retrieved ozone concentration has smoothed the information in the data. Thus, the full-width at half-maximum (FWHM) of these kernels can be considered a measure of the vertical resolution of the retrieved profile. The FWHM of the AVK reveals an altitude resolution that varies from 10 km at 3 hPa (39 km) to 18 km at 0.7 hPa (66 km), indicating that that altitude resolution becomes coarser with increasing altitude as the ozone line width becomes dominated by the Doppler contribution rather than pressure broadening.

The area under the AVK, known as the measurement response and shown by the black line in Fig. 3c, denotes the degree to which the retrieved value at that altitude is driven by the information from the measurement. The solid part of the curve shows

ESSDD
6, 513–540, 2013
Atmospheric ozone above Troll station, Antarctica measured by BAS-MRT
M. Daae et al.

where the measurement response is greater than 0.8, indicating that between 3 hPa and 0.02 hPa (about 38 and 72 km) the retrieved profile has a high degree of independence from the a priori. Outside of this area the measurement response weakens (shown by a dashed curve) and vmr values in this region should be interpreted with caution as the information from the a priori becomes important.

Figure 3d compares a summer noon and a winter midnight O_3 profile. The summer noon profile shows a stratospheric ozone peak of 5 ppmv at 35 km, the mesospheric minimum, and a weak secondary maximum of 1 ppmv at 91 km. The midnight winter profile shows the stratospheric ozone layer which has a similar magnitude to the summer time. The significant change from summer to winter occurs for the secondary maximum and the now apparent tertiary maximum with peak values of 3.2 ppmv and 2.2 ppmv at 93 km and 69 km, respectively.

Figure 4 shows the mesospheric (top panel) and the stratospheric (bottom panel) ozone volume mixing ratio as observed by BAS-MRT over its two years of operation. The black solid line indicates the upper/lower limit of the 0.8 measurement response, indicating that the topside of the stratospheric ozone layer is captured over the whole time period with a magnitude from 3 ppmv to >6 ppmv. The lower mesospheric O_3, and in particular the tertiary maximum that appears in winter, is captured with good confidence for each profile. The tertiary O_3 maximum is observed from fall through spring in both years (2008 and 2009) with a magnitude between 1 ppmv and 3 ppmv, and is more pronounced in the fall than in spring.

The O_3 concentrations during the summertime, which we define as the period when the solar elevation angle stays above 0° throughout a 24 h period (13 November to 28 January), vary between 0 and 1 ppmv near 60 km, and between 0 and 0.3 ppmv near 72 km.

3.3 Error characterization

The standard deviation (1-σ) of the random measurement error of the O_3 retrieval is estimated by propagating the measurement noise on the spectra through the inversion

ESSDD
6, 513–540, 2013

(Rodgers, 2004). The 1-σ total systematic error is estimated by perturbing the atmospheric temperatures, the calibration, the line intensity and the air-broadening parameters with their respective uncertainties. The perturbations will propagate and affect the resulting profile trough the retrieval routine, and the errors are found from the difference to the original set-up. The atmospheric temperature is perturbed by ±5 K, which is the upper limit of the 1-sigma variability of the 20 yr SD-WACCM temperature climatology above Troll. For the estimation of the calibration error we take into account all the uncertainties in the calibration of the radiometer (hot/cold load calibration, standing waves, line of sight, tropospheric correction factor), and impose it as an upper limit of ± 10 % of the tropospheric correction factor. For the spectroscopic parameters we assume the line intensity has an uncertainty of ±2 %, and for the air-broadening parameter we use ±5 % (Rothman et al., 2009). The variability in the a priori is set to 50 % in order to simulate large changes observed in the mesospheric ozone.

We use midnight profiles to characterize the errors of the retrieved O_3 profiles. The estimated errors in vmr are also representative of the noon profiles. The error estimations are displayed in Fig. 5, and show that the random measurement error is within 6 % of the O_3 vmr and the total systematic error is within 9 % at altitudes with a measurement response of at least 0.8. The air-broadening parameter is the largest error up to about 0.1 hPa, peaking at altitudes where the change in brightness temperature with frequency of the O_3 spectra maximizes. The systematic errors given by the temperature, calibration and line-intensity are negligible at all altitudes. The estimation of the a priori sensitivity indicates where and how much the retrieved O_3 profile is sensitive to the a priori. Despite the a priori being perturbed by 50 %, the resulting response is only larger than the systematic error below 2 hPa (6–8 %) and above 0.07 hPa (6–15 %).

ESSDD
6, 513–540, 2013

4 Comparison to Aura/MLS and SD-WACCM

4.1 Aura/MLS

The Earth Observing System (EOS) Aura satellite was launched in July 2004 into a near polar, sun-synchronous orbit with a period of about 100 min. The satellite crosses the equator on the ascending node at about 13:45 UTC ±15 min every day, repeating its ground track every 16 days. The Microwave Limb Sounder (MLS) aboard Aura provides day and night measurements of O_3 from thermal emissions near 240 GHz. Validation of the version 2.2 O_3 data is given by Froidevaux et al. (2008) and reveals about 5–10 % difference in the ozone vmr in the stratosphere and 5–25 % in the mesosphere compared to other satellites. We use the version 3.3 O_3 retrievals which are described by Livesey et al. (2011). The retrieved O_3 profiles cover a pressure range between 215 hPa and 0.02 hPa with a vertical resolution of about 3 km in the stratosphere and about 5 km in the mesosphere. For the comparison we use profiles within ±1° latitude and ±5° longitude with respect to the Troll station (72.5° S, 2.5° E), resulting in 419 days with profiles available at about midnight and/or around 15:00 UTC.

4.2 SD-WACCM

The Whole Atmosphere Community Climate Model (WACCM) is a general circulation model coupled with the Community Atmospheric Model (CAM) chemistry model from the National Center for Atmospheric Research (NCAR). WACCM incorporates wave parameterization, molecular diffusion, and some space weather effects as described by Garcia et al. (2007). It is usually operated as a free-running climatological model, but the Specified Dynamics (SD-WACCM) version is relaxed toward meteorological fields (e.g. temperature, zonal and meridional winds, and surface pressure) from GEOS-5.2 in the troposphere and stratosphere up to approximately 40 km, and then linearly relaxed toward the free-running model from 40 to 50 km (Marsh, 2011; Lamarque et al., 2012). The latitude and longitude resolution of SD-WACCM is 1.9° × 2.5°. Each profile

ESSDD
6, 513–540, 2013

is given at 88 pressure levels with approximately two grid points per scale height, and a corresponding altitude range from the surface to about 150 km. For the comparison we use SD-WACCM midnight profiles at the grid point nearest to Troll station.

4.3 Results

For the following comparisons we generate a set of time-coincident profiles between BAS-MRT and MLS, and BAS-MRT and SD-WACCM. The requirement is that the profiles should be within one hour of each other, resulting in a set of 582 profiles for MLS and 630 profiles for SD-WACCM. Since both MLS and SD-WACCM have a better altitude resolution than BAS-MRT, we convolve their profiles with the AVK from the BAS-MRT data inversion.

4.4 Temporal variations

To address the reliability of the temporal variations resolved by BAS-MRT we compare co-incident vmr values at three independent pressure levels (0.21, 0.39 and 0.04 hPa) corresponding to the upper stratosphere, near the stratopause, and the middle mesosphere (which includes the tertiary maximum). The correlation between MLS and BAS-MRT and SD-WACCM and BAS-MRT is carried out between the datasets for the entire measurement period. However, due to the large winter to summer variations of the ozone concentrations, particularly in the mesosphere, the correlation analysis is also carried out for the winter and summer seasons separately. We only report correlation coefficients that are statistically significant at greater than the 95 % confidence level. For convenience in the discussion of the correlation coefficients, we refer to correlations ≥ 0.7 as strong, from 0.3 to 0.7 as moderate, and < 0.3 as weak. We first discuss temporal variations on timescales larger than 20 days, and then variations on timescales shorter than 20 days.

The left panels in Fig. 6 show the temporal behavior for all available co-incident data points as well as for the low frequency variations (timescales > 20 days) for each of the

ESSDD
6, 513–540, 2013

Atmospheric ozone above Troll station, Antarctica measured by BAS-MRT

M. Daae et al.

co-incident SD-WACCM, MLS and BAS-MRT data sets at three independent pressure levels. It indicates that, in general, observations from BAS-MRT agree well with the vmr values from both MLS and SD-WACCM. The right panel in Fig. 6 shows the correlation coefficients between the low-pass filtered data of BAS-MRT and both MLS and SD-WACCM. Discussing the comparison between MLS and BAS-MRT first, it can be seen that the overall correlation (red solid line) is strong at all altitudes. This correlation is largely dominated by the seasonal variations, particularly in the middle mesosphere (top left panel in Fig. 6). However, the seasonal effect is smaller in the stratosphere (bottom left panel in Fig. 6) and the correlation reflects intraseasonal dynamical variations. In winter, the strong correlation (red dashed line) is preserved at all altitudes indicating that dynamical and chemical changes on time-scales larger than 20 days are well captured by BAS-MRT. In the summer the correlation (red dotted line) is still strong in the stratosphere but weakens with increasing altitude as we enter the mesospheric minimum, even though BAS-MRT measures above its random noise-level. We believe this is due to the random noise in single MLS profiles (with an approximate integration time of < 90 s) gradually becoming larger than the measured vmr values in this region (Fig. 8).

The right panel in Fig. 6 also shows that the overall correlation (green solid line) of the low frequency variations between SD-WACCM and BAS-MRT is generally strong. It weakens around the stratopause, which is where the minimum between the stratospheric ozone layer and the tertiary maximum occurs. Due to the strong concentration gradients in this region, small deviations in the maxima locations would lead to larger deviations and poorer correlation between the ozone variations. In winter, the correlation (green dashed line) stays moderate at all pressure levels. The summer correlation coefficients (green dotted line) are strong in the stratosphere but, they do not reveal a consistent picture at higher altitudes corresponding to where SD-WACCM is no longer driven by GEOS-5.2 data. However, the general agreement in the comparison between BAS-MRT and both MLS and SD-WACCM indicates that the atmospheric variability on time-scales exceeding 20 days is well captured by BAS-MRT.

ESSDD
6, 513–540, 2013

The left panels in Fig. 7 show the higher frequency vmr variations for SD-WACCM, MLS and BAS-MRT for the same pressure levels as above (Fig. 6). The vmr variations are found by subtracting the low-pass filtered data from their respective datasets, which effectively creates a high-pass filter for time scales shorter than 20 days (Kennedy, 1980). The result indicates variations of similar magnitude for all the data sets in the stratosphere and around the stratopause, while in the mesosphere MLS observes larger variations than BAS-MRT and SD-WACCM, particularly during summer. The right panel in Fig. 7 shows the calculated correlation coefficients between the high-pass filtered data of BAS-MRT and both MLS and SD-WACCM. Discussing the result between MLS and BAS-MRT first, it can be seen that the overall shot-term correlation is strong in both the stratosphere and mesosphere, indicating that atmospheric variations on time scales shorter than 20-days are well captured by BAS-MRT. Looking closer at the vmr variations in winter, the correlation stays strong in the stratosphere but becomes moderate in the mesosphere. The summer time vmr variations correlate moderately in the stratosphere, but since the vmr values in the summertime fall below the random noise level of MLS, the correlation becomes, as expected, insignificant. Despite SD-WACCM being poorly suited for characterizing short term variations in the ozone at a single location and time, the overall correlation with BAS-MRT is still moderate/strong at around 40 km where it is driven by the reanalysis data. As SD-WACCM is linearly relaxed to the free running mode by 50 km, the correlation weakens and becomes insignificant in the middle mesosphere.

4.5 Comparison of profiles

The comparison between profiles of BAS-MRT and Aura MLS, and between BAS-MRT and SD-WACCM, are carried out following the procedures by Stiller et al. (2012). The left panels in Fig. 8 shows the mean of the O_3 profiles from BAS-MRT, MLS and SD-WACCM at co-incident times. In general there is a very good agreement between the profiles, with MLS showing slightly higher values at about 3 hPa than SD-WACCM and BAS-MRT. The middle panel of Fig. 8 displays the average difference (bias) and

ESSDD
6, 513–540, 2013

standard error between the profiles together with the estimated systematic error of BAS-MRT. This confirms that biases between the instruments and models are within the 1-sigma accuracy (systematic error) estimate of BAS-MRT at all altitudes above 2 hPa. Even though there appears to be a significant low bias of BAS-MRT relative to MLS below this level, the instruments agree to within the combined instrumental accuracy estimates (Livesey et al., 2011). Thus, there is no significant bias between BAS-MRT and MLS, or between BAS-MRT and SD-WACCM at the combined accuracy level.

The right panel of Fig. 8 displays the standard deviation of the difference between the profiles, together with both the individual and combined random errors of BAS-MRT and MLS. The standard deviation of the difference between MLS and BAS-MRT varies between 0.15 and 0.3 ppmv, which is always less than the combined random error estimates of the two instruments. This total random error above 45 km is chiefly due to MLS, whose single-profile random error is larger than BAS-MRT profiles derived from continuous observations integrated over 1 h. However, in this region the total random error is much larger than the standard deviation of the differences between the profiles, indicating that the MLS random error may be overestimated here. Compared to SD-WACCM the random errors of BAS-MRT can not alone account for the random differences between the profiles. Unfortunately errors of SD-WACCM are not provided along with their profiles. However, the similar shape of the standard deviation of the difference between BAS-MRT and the SD-WACCM and MLS may indicate that there is a contribution to the random error in BAS-MRT that is not accounted for by the retrieval routine.

5 Conclusions

This paper describes and presents the O_3 measurements from the British Antarctic Survey's microwave radiometer stationed at Troll, Antarctica from February 2008 through January 2010. The retrieval of the hourly O_3 vmr values resulted in 13 648 profiles over 675 days (of 715 possible days) with an average of about 20 profiles per day. The retrieved profiles cover the pressure range from 3 to 0.02 hPa (approximately 38–72 km) which includes the topside of the stratospheric ozone layer and the bottom side of the tertiary maximum in the mesosphere. Comparison of BAS-MRT to Aura/MLS and SD-WACCM shows a good correlation indicating that the atmospheric variability on time-scales both larger and shorter than 20 days is well captured by BAS-MRT. Taken seasonally, a weaker correlation is found for both the long-term and short-term variations in summer when most of the vmr values are below the random noise level in Aura/MLS. At all altitudes the comparison of O_3 profiles between BAS-MRT and MLS and SD-WACCM reveals no significant bias in measured vmr outside the combined systematic errors of the instruments. The dataset presented here are available for public use and can be downloaded from the UK's Polar Data Center at http://doi.org/nc3.

The results presented in this paper indicate that the retrieved O_3 profiles from BAS-MRT are well suited for studies of the upper stratospheric and middle mesospheric ozone, including the tertiary maximum. The data quality will allow short (∼ hours), seasonal and inter-seasonal O_3 variations to be observed, including effects from transient events such as particle precipitation. The instrument is continuing polar observations from Halley (75°35′ S, 26°39′ W), Antarctica from the Austral autumn 2013 season onwards, measuring middle atmospheric CO, NO and O_3 while viewing toward the South Pole.

Acknowledgements. We gratefully thank Ole Martin Christensen for help on the implementation and understanding of ARTS 2, and Stephan Thomas Kral with valuable discussions on interpretation of the intercomparison. We thank Dan Marsh and Anne K. Smith for providing SD-WACCM data used in the ozone retrievals and in the comparison. We thank Mark Clilverd at BAS, Kim Holmén at the Norwegian Polar Institute (NPI) and Paul Hartogh at Max Planck Institute (MPI, Germany) for their support of the BAS microwave radiometer. We also thank the Troll station over-wintering engineers Atle Markussen, Asbjorn Djupdal, and Tore Dahl as well as David Maxfield and Paul Breen at BAS for their help. Corinne Straub was funded by the Norwegian Polar Institute Antarctic Program under the grant Observations of carbon monoxide and ozone in the Antarctic and Arctic: implications for the Inter-hemispheric coupling of

vertical motions. The BAS microwave radiometer project is funded by the Natural Environment Research Council (UK).

References

Daae, M., Espy, P., Nesse Tyssøy, H., Newnham, D., Stadsnes, J., and Søraas, F.: The effect of energetic electron precipitation on middle mesospheric night-time ozone during and after a moderate geomagnetic storm, Geophys. Res. Lett., 39, L21811, doi:10.1029/2012GL053787, 2012. 515, 516

Demissie, T. D., Kleinknecht, N. H., Hibbins, R. E., Espy, P. J., and Straub, C.: Quasi-16 day period oscillations observed in mdidle atmospheric ozone and temperature in Antarctica, Ann. Geophys., in press, 2013. 516

Dicke, R. H. and Beringer, R.: Microwave radiation from the sun and moon, Astrophys. J., 103, 375–276, 1946. 517

Eriksson, P., Jiménez, C., and Buehler, S. A.: Qpack, a general tool for instrument simulation and retrieval work, J. Quant. Spectrosc. Ra., 91, 47–64, doi:10.1016/j.jqsrt.2004.05.050, 2005. 518

Eriksson, P., Buehler, S., Davis, C., Emde, C., and Lemke, O.: ARTS, the atmospheric radiative transfer simulator, version 2, J. Quant. Spectrosc. Ra., 112, 1551–1558, doi:10.1016/j.jqsrt.2011.03.001, 2011. 518

Espy, P., Hartogh, P., and Holmén, K.: A microwave radiometer for the remote sensing of nitric oxide and ozone in the middle atmosphere, in: Remote Sensing of Clouds and the Atmosphere XI, Proc. SPIE, vol. 6362, doi:10.1117/12.688953, 2006. 517

Forkman, P., Christensen, O. M., Eriksson, P., Urban, J., and Funke, B.: Six years of mesospheric CO estimated from ground-based frequency-switched microwave radiometry at 57° N compared with satellite instruments, Atmos. Meas. Tech., 5, 2827–2841, doi:10.5194/amt-5-2827-2012, 2012. 517

Froidevaux, L., Jiang, Y. B., Lambert, A., Livesey, N. J., Read, W. G., Waters, J. W., Browell, E. V., Hair, J. W., Avery, M. A., McGee, T. J., Twigg, L. W., Sumnicht, G. K., Jucks, K. W., Margitan, J. J., Sen, B., Stachnik, R. A., Toon, G. C., Bernath, P. F., Boone, C. D., Walker, K. A., Filipiak, M. J., Harwood, R. S., Fuller, R. A., Manney, G. L., Schwartz, M. J., Daffer, W. H., Drouin, B. J., Cofield, R. E., Cuddy, D. T., Jarnot, R. F., Knosp, B. W., Perun,

ESSDD
6, 513–540, 2013

Atmospheric ozone above Troll station, Antarctica measured by BAS-MRT

M. Daae et al.

V. S., Snyder, W. V., Stek, P. C., Thurstans, R. P., and Wagner, P. A.: Validation of Aura Microwave Limb Sounder stratospheric ozone measurements, J. Geophys. Res., 113, D15S20, doi:10.1029/2007JD008771, 2008. 522

Garcia, R. R., Marsh, D. R., Kinnison, D. E., Boville, B. A., and Sassi, F.: Simulation of secular trends in the middle atmosphere, 1950–2003, J. Geophys. Res., 112, D09301, doi:10.1029/2006JD007485, 2007. 519, 522

Hartogh, P. and Hartmann, G. K.: A high-resolution chirp transform spectrometer for microwave measurements, Meas. Sci. Technol., 1, 592, doi:10.1088/0957-0233/1/7/008, 1990. 517

Hartogh, P., Jarchow, C., Sonnemann, G. R., and Grygalashvyly, M.: On the spatiotemporal behavior of ozone within the upper mesosphere/mesopause region under nearly polar night conditions, J. Geophys. Res., 109, D18303, doi:10.1029/2004JD004576, 2004. 515

Hays, P. B. and Roble, R. G.: Observation of mesospheric ozone at low latitudes, Planet. Space Sci., 21, 273–279, 1973. 515

Jackman, C. H., Marsh, D. R., Vitt, F. M., Garcia, R. R., Randall, C. E., Fleming, E. L., and Frith, S. M.: Long-term middle atmospheric influence of very large solar proton events, J. Geophys. Res., 114, D11304, doi:10.1029/2008JD011415, 2009. 515

Kennedy, J. S.: Comments on “On detrending and smoothing random data” by A. J. Owens, J. Geophys. Res., 85, 219–220, doi:10.1029/JA085iA01p00219, 1980. 525

Lamarque, J.-F., Emmons, L. K., Hess, P. G., Kinnison, D. E., Tilmes, S., Vitt, F., Heald, C. L., Holland, E. A., Lauritzen, P. H., Neu, J., Orlando, J. J., Rasch, P. J., and Tyndall, G. K.: CAM-chem: description and evaluation of interactive atmospheric chemistry in the Community Earth System Model, Geosci. Model Dev., 5, 369–411, doi:10.5194/gmd-5-369-2012, 2012. 519, 522

Livesey, N. J., Read, W. G., Froidevaux, L., Lambert, A., Manney, G. L., Pumphrey, H. C., Santee, M. L., Schwartz, M. J., Wang, S., Cofield, R. E., Cuddy, D. T., Fuller, R. A., Jarnot, R. F., Jiang, J. H., Knosp, B. W., Stek, P. C., Wagner, P. A., and Wu, D. L.: EOS/MLS Version 3.3. Level 2 data quality and description document, Tech. Rep. Jet Propulsion Laboratory, D-33 509, 2011. 522, 526

Marsh, D.: Chemical-dynamical coupling in the mesosphere and lower thermosphere, vol. 2, Springer, Aeronomy of the Earth's Atmosphere and Ionosphere Edn., doi:10.1007/978-94-007-0326-1, 2011. 519, 522

ESSDD
6, 513–540, 2013

Atmospheric ozone above Troll station, Antarctica measured by BAS-MRT

M. Daae et al.

Marsh, D., Smith, A., Brasseur, G., Kaufmann, M., and Grossmann, K.: The existence of a tertiary ozone maximum in the high-latitude middle mesosphere, Geophys. Res. Lett., 28, 4531–4534, 2001. 515

McDermid, I. S., Bergwerff, J. B., Bodeker, G., Boyd, I. S., Brinksma, E. J., Connor, B. J., Farmer, R., Gross, M. R., Kimvilakani, P., Matthews, W. A., McGee, T. J., Ormel, F. T., Parrish, A., Singh, U., Swart, D. P. J., and Tsou, J. J.: OPAL: Network for the Detection of Stratospheric Change ozone profiler assessment at Lauder, New Zealand 1. Blind intercomparison, J. Geophys. Res., 103, 28683–28692, doi:10.1029/98JD02706, 1998. 516

Muscari, G., Cesaroni, C., Fiorucci, I., Smith, A. K., Froidevaux, L., and Mlynzak, M.: Strato-mesospheric ozone measurements using ground-based millimeter-wave spectroscopy at Thule, Greenland, J. Geophys. Res., 117, D07307, doi:10.1029/2011JD016863, 2012. 515

Nemuc, A. and De Zafra, R. L.: Ozone profiles over the South Pole from ground-based retrievals and satellite data, J. Optoelectron. Adv. Mater., 9, 3533–3540, 2007. 516

Newnham, D. A., Espy, P. J., Clilverd, M. A., Rodger, C. J., Seppälä, A., Maxfield, D. J., Hartogh, P., Holmén, K., and Horne, R. B.: Direct observations of nitric oxide produced by energetic electron precipitation into the Antarctic middle atmosphere, Geophys. Res. Lett., 38, L20104, doi:10.1029/2011GL048666, 2011. 516

Orte, P. F., Salvador, J., Wolfram, E., D'Elia, R., Nagahama, T., Kojima, Y., Tanada, R., Kuwahara, T., Morihira, A., Quel, E., and Mizuno, A.: Millimeter wave radiometer installation in Rio Gallegos, southern Argentina, in: Int. Conf. on Applications of Opt. and Photonics, edited by: Costa, M. F. M., Vol. 8001 of Proceedings of SPIE, doi:10.1117/12.894578, 2011. 516

Palm, M., Hoffmann, C. G., Golchert, S. H. W., and Notholt, J.: The ground-based MW radiometer OZORAM on Spitsbergen – description and status of stratospheric and mesospheric O_3-measurements, Atmos. Meas. Tech., 3, 1533–1545, doi:10.5194/amt-3-1533-2010, 2010. 515

Parrish, A.: Millimeter-wave remote sensing of ozone and trace constituents in the stratosphere, Proc. IEEE, 82, 1915–1929, 1994. 517

Randall, C. E., Harvey, V. L., Singleton, C. S., Bernath, P. F., Boone, C. D., and Kozyra, J. U.: Enhanced NO_x in 2006 linked to strong upper stratospheric Arctic vortex, Geophys. Res. Lett., 33, D08308, doi:10.1029/2006GL027160, 2006. 515

Rodgers, C. D.: Inverse methods for atmospheric sounding: Theory and Practice, vol. 2 of Series on Atmospheric, Ocean and Planetary Physics, World Scientific, 2004. 518, 519, 521

ESSDD
6, 513–540, 2013

Atmospheric ozone above Troll station, Antarctica measured by BAS-MRT

M. Daae et al.

Rothman, L., Gordon, I., Barbe, A., Benner, D., Bernath, P., Birk, M., Boudon, V., Brown, L., Campargue, A., Champion, J.-P., Chance, K., Coudert, L., Dana, V., Devi, V., Fally, S., Flaud, J.-M., Gamache, R., Goldman, A., Jacquemart, D., Kleiner, I., Lacome, N., Lafferty, W., Mandin, J.-Y., Massie, S., Mikhailenko, S., Miller, C., Moazzen-Ahmadi, N., Naumenko, O., Nikitin, A., Orphal, J., Perevalov, V., Perrin, A., Predoi-Cross, A., Rinsland, C., Rotger, M., Simeckova, M., Smith, M., Sung, K., Tashkun, S., Tennyson, J., Toth, R., Vandaele, A., and Auwera, J. V.: The HITRAN 2008 molecular spectroscopic database, J. Quant. Spectrosc. Ra., 110, 533–572, doi:10.1016/j.jqsrt.2009.02.013, 2009. 518, 521

Solomon, S., Crutzen, P. J., and Roble, R. G.: Photochemical Coupling Between the Thermosphere and the Lower Atmosphere 1. Odd Nitrogen From 50 to 120 km, J. Geophys. Res., 87, 7206–7220, 1982. 515

Sonnemann, G., Hartogh, P., Jarchow, C., Grygalashvyly, M., and Berger, U.: On the winter anomaly of the night-to-day ratio of ozone in the middle to upper mesosphere in middle to high latitudes, Adv. Space Res., 40, 846–854, doi:10.1016/j.asr.2007.01.039, 2007. 515

Stiller, G. P., Kiefer, M., Eckert, E., von Clarmann, T., Kellmann, S., García-Comas, M., Funke, B., Leblanc, T., Fetzer, E., Froidevaux, L., Gomez, M., Hall, E., Hurst, D., Jordan, A., Kämpfer, N., Lambert, A., McDermid, I. S., McGee, T., Miloshevich, L., Nedoluha, G., Read, W., Schneider, M., Schwartz, M., Straub, C., Toon, G., Twigg, L. W., Walker, K., and Whiteman, D. N.: Validation of MIPAS IMK/IAA temperature, water vapor, and ozone profiles with MOHAVE-2009 campaign measurements, Atmos. Meas. Tech., 5, 289–320, doi:10.5194/amt-5-289-2012, 2012. 525

Straub, C., Espy, P. J., Hibbins, R. E., and Newnham, D. A.: Mesospheric CO above Troll station, Antarctica observed by a ground based microwave radiometer, Earth Syst. Sci. Data, 5, 199–208, doi:10.5194/essd-5-199-2013, 2013. 516, 517

Turunen, E., Verronen, P. T., Seppälä, A., Rodger, C. J., Clilverd, M. A., Tamminen, J., Enell, C.-F., and Ulich, T.: Impact of different energies of precipitating particles on NO_x generation in the middle and upper atmosphere during geomagnetic storms, J. Atmos. Sol.-Terr. Phy., 71, 1176–1189, 2009. 515

Verronen, P. T., Rodger, C. J., Clilverd, M. A., and Wang, S.: First evidence of mesospheric hydroxyl response to electron precipitation from the radiation belts, J. Geophys. Res., 116, D07307, doi:10.1029/2010JD014965, 2011. 515

Villanueva, G. L. and Hartogh, P.: The high resolution chirp transform spectrometer for the SOFIA-GREAT instrument, Exp. Astron., 18, 77–91, doi:10.1007/s10686-005-9004-3, 2004. 517

Villanueva, G. L., Hartogh, P., and Reindl, L.: A digital dispersive matching network for SAW devices in chirp transform spectrometers, IEEE Trans. Microw. Theory Tech., 54, 1415–1424, doi:10.1109/TMTT.2006.871244, 2006. 517

ESSDD

6, 513–540, 2013

Atmospheric ozone above Troll station, Antarctica measured by BAS-MRT

M. Daae et al.

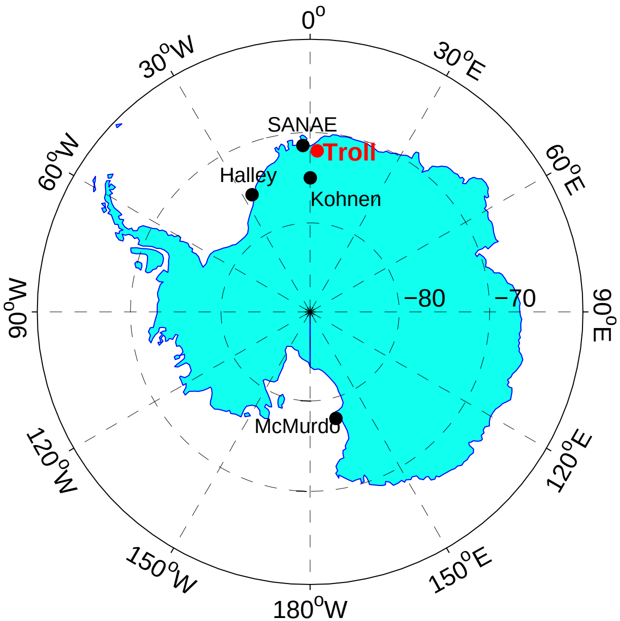

Fig. 1. Location of BAS-MRT at the Troll research facility in Antarctica (72° S, 2.5° E). The instrument's view direction is 288° azimuth (toward SANAE), with a zenith angle of 60°.

ESSDD
6, 513–540, 2013

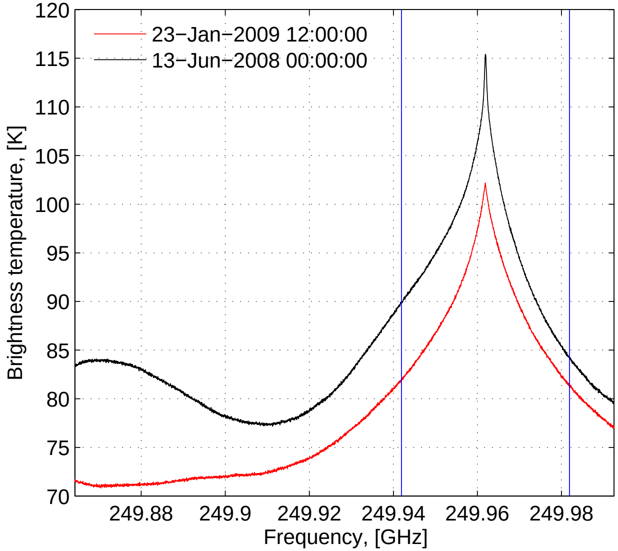

Fig. 2. Noon summer (red) and midnight winter (black) calibrated atmospheric spectra. The blue vertical lines indicate the frequency range of the spectra used in the O_3 retrieval.

ESSDD
6, 513–540, 2013

ESSDD
6, 513–540, 2013
Atmospheric ozone above Troll station, Antarctica measured by BAS-MRT
M. Daae et al.

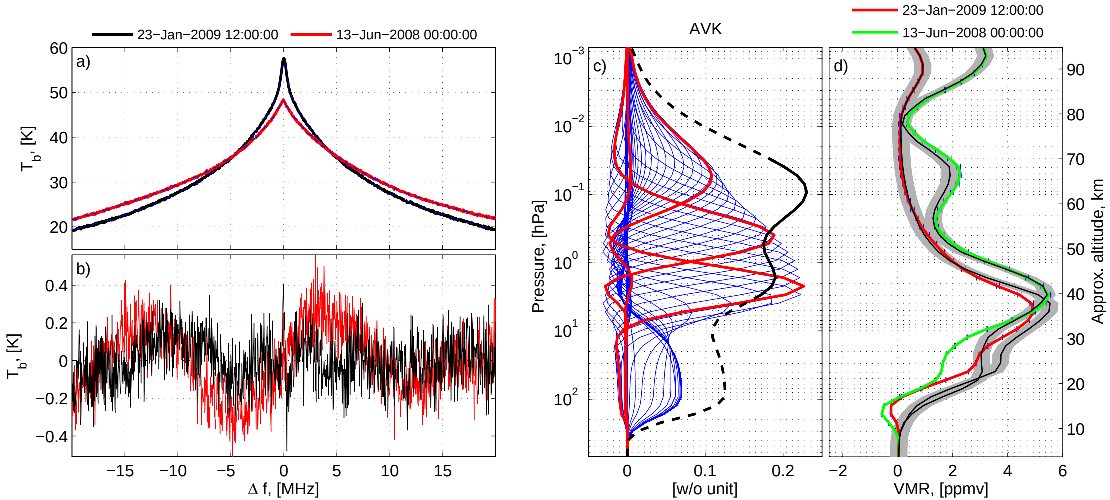

Fig. 3. Top left panel **(a)**: tropospheric- and baseline-corrected spectra for noon summer (red) and midnight winter (black), along with the fitted spectra (dashed blue). Bottom left panel **(b)**: residuals between the corrected spectra and the fitted spectra for noon summer (red) and midnight winter (black). Middle panel **(c)**: the AVK from the retrieval, solid red lines are the AVK at 2.21 hPa, 0.39 hPa and 0.04 hPa (approximately 41 km, 54 km and 71 km). The black line is the measurement response from the AVK divided by 5, where the solid (dashed) part indicates the area of at least (less than) 0.8 measurement response. Right panel **(d)**: summer noon (red) and midnight winter profiles (green) with their barely visible random measurement error (blue error bars). The thin black solid line is the a priori with the grey shade showing the 1-σ standard deviation of the a priori used in the retrieval.

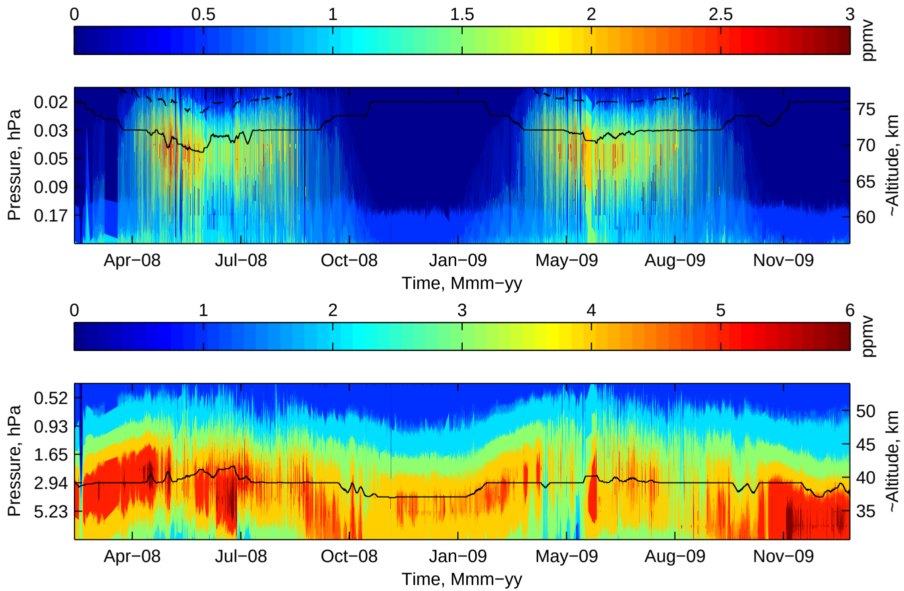

Fig. 4. Top panel: BAS-MRT ozone data showing the mesospheric ozone. The solid black line indicates the upper limit of the 0.8 measurement response, while the dashed black line indicates the upper limit of 0.5 measurement response. Bottom panel: stratospheric ozone observations from BAS-MRT. The solid black line indicates the lower limit of 0.8 measurement response.

ESSDD

6, 513–540, 2013

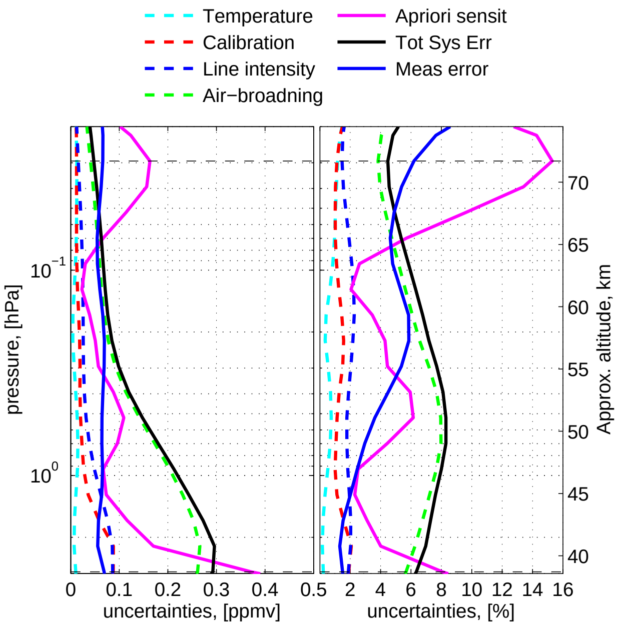

Fig. 5. Error estimations of the BAS-MRT O_3-retrieval: the black solid line shows the total systematic error, which is the root-sum-square of the dashed lines. The blue solid line is the random measurement error. The magenta solid line is the a priori sensitiviy. Dashed horizontal black lines indicate the upper/lower limit of the 0.8 measurement response. Left panel: uncertainties in ppmv representing all times. Right panel: uncertainties in % of midnight O_3-profile.

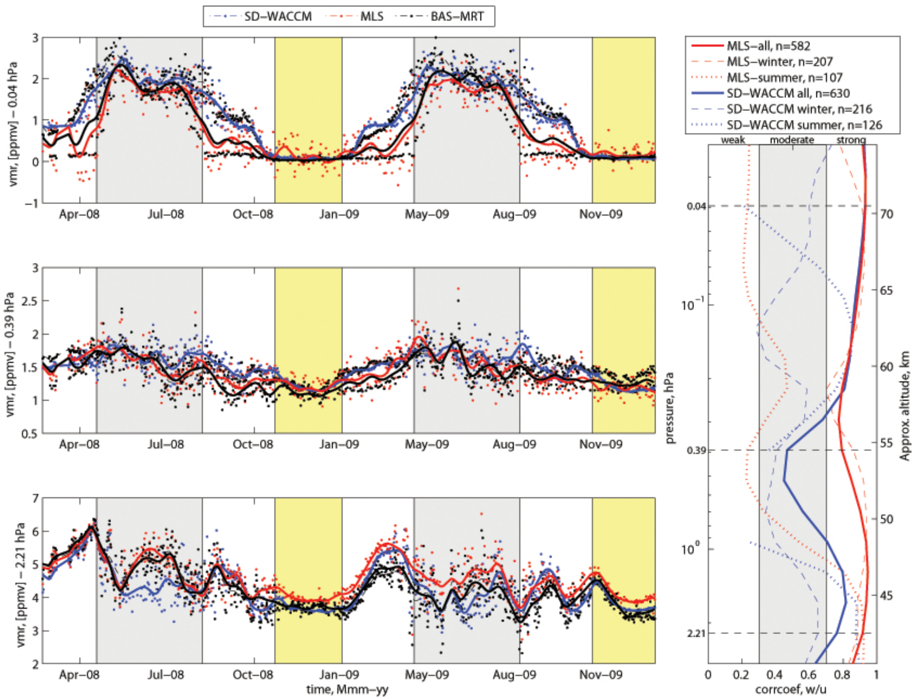

Fig. 6. Time series of co-incident data between MLS and BAS-MRT, and between SD-WACCM and BAS-MRT at three independent pressure levels. Left panels: dots marks the data points for the datasets, solid lines low-pass filtered data with a 20-day cut-off. Grey shade marks winter time defined by solar elevation angle below -30°, yellow shade marks summer time defined by solar elevation angle above 0°. Right panel: calculated correlation coefficients for the low-pass filtered data between BAS-MRT and MLS, and BAS-MRT and SD-WACCM. Thick solid line is for the entire measurement period, while dashed and dotted are correlation coefficients for the winter and summer respectively. The number of correlated data points (n) is listed in the legend for the respective calculations.

ESSDD
6, 513–540, 2013

Atmospheric ozone above Troll station, Antarctica measured by BAS-MRT

M. Daae et al.

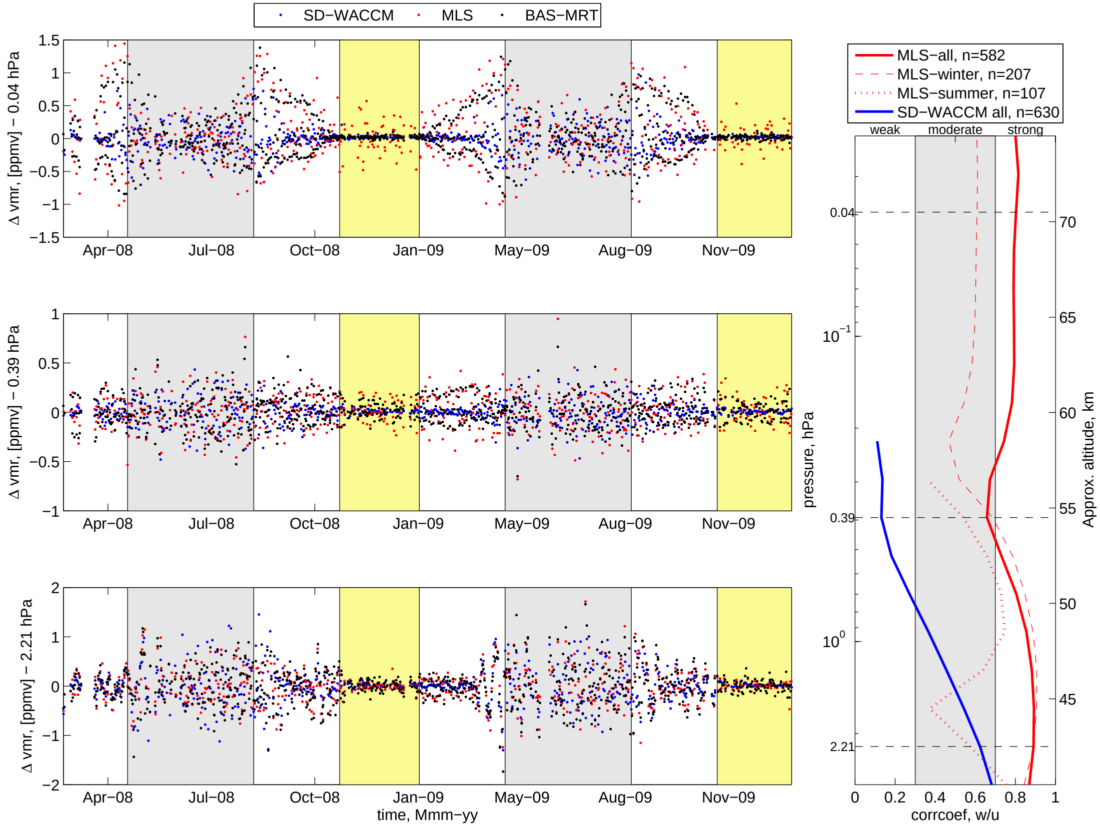

Fig. 7. Same as Fig. 6, but for high-passed filter data with a 20-day cut-off (low-pass filter subtracted from the data).

ESSDD
6, 513–540, 2013

Atmospheric ozone above Troll station, Antarctica measured by BAS-MRT

M. Daae et al.

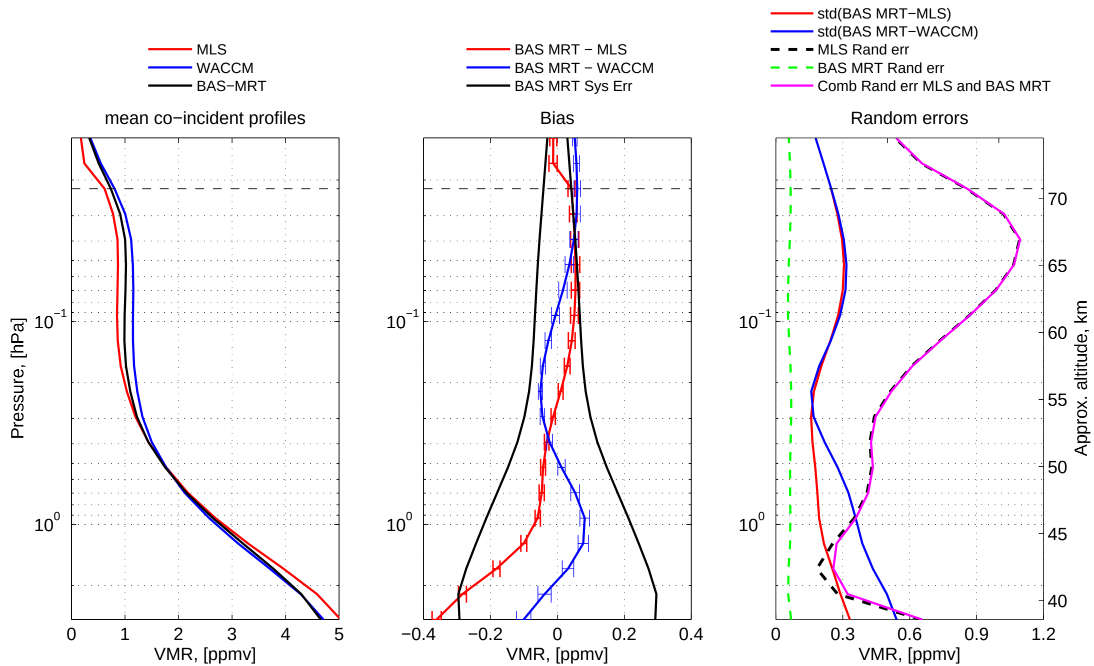

Fig. 8. Intercomparison between BAS-MRT, MLS and SD-WACCM using co-incident profiles: left panel: mean of midnight profiles. Middle panel: the bias with the 1-σ of the standard error of the bias. The black solid line is the $\pm$1-σ of the total systematic error of BAS-MRT. Right panel: standard deviation of the bias between the co-incident profiles of BAS-MRT to MLS (red) and SD-WACCM (blue). The combined (magenta) and individual (dashed) random errors of MLS and BAS-MRT for midnight values are also shown.

ESSDD
6, 513–540, 2013

Atmospheric ozone above Troll station, Antarctica measured by BAS-MRT

M. Daae et al.